Contrasting magnetic and magnetoelectric properties of LuMWO6 (M = Fe and Cr): Role of spin frustration and noncollinear magnetic structure

Swarnamayee Mishra, Premakumar Yanda, Fabio Orlandi, Pascal Manuel, Hyun-Joo Koo, Myung-Hwan Whangbo, and A. Sundaresan

Contrasting magnetic and magnetoelectric properties of LuMWO$_6$ (M = Fe and Cr): Role of spin frustration and noncollinear magnetic structure

Swarnamayee Mishra [●],[1] Premakumar Yanda [●],[1] Fabio Orlandi [●],[2] Pascal Manuel,[2] Hyun-Joo Koo [●],[3] Myung-Hwan Whangbo,[3,4] and A. Sundaresan [●][1,*]

[1]*School of Advanced Materials, and Chemistry and Physics of Materials Unit, Jawaharlal Nehru Centre for Advanced Scientific Research, Jakkur, Bangalore 560064, India*
[2]*ISIS Facility, Rutherford Appleton Laboratory, Harwell Campus, Didcot OX11 0QX, United Kingdom*
[3]*Department of Chemistry and Research Institute for Basic Sciences, Kyung Hee University, Seoul 02447, Republic of Korea*
[4]*Department of Chemistry, North Carolina State University, Raleigh, North Carolina 27695-8204, USA*

We report the magnetic and magnetoelectric properties of two isostructural polar compounds LuMWO$_6$ (M = Fe and Cr) that were synthesized at high pressure and high temperatures. Both compounds have a polar orthorhombic aeschynite-type structure (space group $Pna2_1$) with the ordered M^{3+} and W^{6+} ions. Magnetization measurements show that the Fe^{3+} spins in LuFeWO$_6$ and Cr^{3+} spins in LuCrWO$_6$ exhibit antiferromagnetic (AFM) ordering at T_N = 11.8 and 19.2 K, respectively. Powder neutron diffraction analysis at 1.5 K reveals that LuFeWO$_6$ has a noncollinear AFM structure with $\mathbf{k}$ = (0, $\frac{1}{2}$, $\frac{1}{2}$), whereas LuCrWO$_6$ has a collinear AFM arrangement with $\mathbf{k}$ = (0, 0, 0). The noncollinear AFM structure in LuFeWO$_6$ causes an additional electric polarization, whereas the collinear magnetic order in LuCrWO$_6$ does not. Our density functional theory calculations indicate that LuFeWO$_6$ exhibits spin frustration, which is absent in LuCrWO$_6$. This finding suggests that the induced electric polarization at T_N in LuFeWO$_6$ occurs due to a noncollinear spin structure resulting from magnetic frustration.

I. INTRODUCTION

Multiferroics can be classified into three types based on their ferroelectric polarization and magnetic ordering behavior. In type-I multiferroics, the ferroelectric polarization occurs at high temperatures due to structural distortion, while magnetic ordering occurs at low temperatures, resulting in weak coupling between the electric polarization and magnetic ordering [1–3]. Type-II multiferroics are centrosymmetric in the paramagnetic state, but their magnetic ordering breaks the inversion symmetry, inducing electric polarization and giving rise to a strong coupling between the electric and magnetic orders [1–7]. Type-III multiferroics are pyroelectric polar magnets that undergo a pyroelectric-to-ferroelectric transition at the magnetic ordering temperature [8–19]. In contrast to type-I multiferroics, where the ferroelectric distortion arises from the second-order Jahn-Teller effect or geometric distortion, type-III multiferroics typically have their inversion symmetry broken by chemical ordering [19]. Additionally, polar magnetic oxides exhibit behavior like type-II multiferroics below the magnetic ordering temperature. However, they differ in that they do not require complex magnetic structures to induce electric polarization at the magnetic ordering temperature. Several compounds such as Ni$_3$TeO$_6$ [20], CaBaCo$_4$O$_7$ [11], M_2Mo$_3$O$_8$ (M = Fe, Mn, and Co) [12–15], $AA'BB'$O$_6$ (A = alkali metal, A' = rare-earth, B = divalent transition metal, and B' = hexavalent transition metal) [18,21], and RFeWO$_6$

(R = rare-earth cations) [17,22,23] have been identified as type-III multiferroics. These compounds exhibit changes or additional polarization below the magnetic ordering temperatures, indicating a strong magnetoelectric coupling. For example, Co$_2$Mo$_3$O$_8$ [15,24] and Fe$_2$Mo$_3$O$_8$ [12,13] exhibit electric polarization at their collinear magnetic ordering, and NaYNiWO$_6$ exhibits additional polarization below the incommensurate spin-density-wave state at 20 K and the collinear antiferromagnetic (AFM) structure at 18 K [21,25].

The compounds in the ordered aeschynite family RMWO$_6$ (R = rare-earth, M = Fe, Cr, and V) [17,22,23,26–32] crystallize in an orthorhombic structure with the polar space group $Pna2_1$, where the transition metal ions M^{3+} and W^{6+} form an ordered arrangement. These compounds can be considered an ordered derivative of the centrosymmetric ($Pnma$) parent compound CaTa$_2$O$_6$ [33]. Ghara *et al.* [17] observed the emergence of a switchable additional polarization at the magnetic ordering temperatures in polycrystalline samples of RFeWO$_6$ (R = Dy, Eu, Tb, and Y). Neutron diffraction studies on DyFeWO$_6$ confirmed a commensurate noncollinear arrangement of the Fe^{3+} and Dy^{3+} spins. The latter has a propagation vector $\mathbf{k}$ = (0, $\frac{1}{2}$, $\frac{1}{2}$) and magnetic space group C_ac, which is consistent with the observation of spontaneous polarization below the AFM ordering temperature (T_N = 18 K) [17]. Adnani *et al.* [23] and Yanda *et al.* [22] reported magnetoelectric multiferroicity in the polar compounds HoFeWO$_6$ and RFeWO$_6$ (R = Sm, Gd, Er, and Tm) where additional polarization was induced at the AFM ordering temperature. In contrast, the Cr-containing isostructural compounds RCrWO$_6$ (R = Dy and Ho) did not exhibit additional polarization at

*sundaresan@jncasr.ac.in

the magnetic ordering temperature, indicating that the absence of spin-induced polarization in $R\text{CrWO}_6$ (R = Dy and Ho) is due to the collinear AFM structure of the Cr spins [28,30]. However, the spin arrangements of the rare-earth ions in both DyCrWO_6 and HoCrWO_6 are noncollinear and do not induce an additional polarization. Therefore, it was suggested that the noncollinear AFM spin structure of Fe^{3+} ions be responsible for additional electric polarization and multiferroicity [30].

In this paper, the magnetic and multiferroic properties of two isostructural compounds LuFeWO_6 and LuCrWO_6 were investigated in the polycrystalline form. The aim was to understand the origin of additional polarization occurring at T_N and to evaluate the spin-exchange interactions using density functional theory (DFT) calculations. It was found that LuFeWO_6, which is polar along the c-axis direction, undergoes AFM ordering at $T_N = 11.8$ K, accompanied by a dielectric anomaly and an additional electric polarization (ΔP). On the other hand, LuCrWO_6 with Cr^{3+} ions order AFM at $T_N = 19.2$ K, but there is no sign of induced electric polarization at and below the AFM ordering temperature. Our DFT calculations show that the AFM structure of LuFeWO_6 is spin frustrated, but that of LuCrWO_6 is not. Thus, the change in polarization in LuFeWO_6 at its AFM ordering arises because of the noncollinear magnetic structure resulting from spin frustration in the Fe^{3+} ion lattice. In this paper, we provide insight into the relationship between spin frustration and the multiferroic properties of polar compounds.

II. EXPERIMENTAL DETAILS

Polycrystalline samples of $\text{Lu}M\text{WO}_6$ (M = Fe and Cr) have been synthesized using a two-step solid-state reaction. In the first step, the compounds $\text{Lu}M\text{O}_3$ were prepared from a finely ground mixture of stoichiometric amounts of Lu_2O_3 and $M_2\text{O}_3$ and heated at the final temperature of $1300\,^\circ\text{C}$ for 12 h with several intermediate grindings. In the second step, $\text{Lu}M\text{O}_3$ and WO_3 powders were mixed in the appropriate ratio and treated at high pressure (4.5 GPa) and high temperature ($1000\,^\circ\text{C}$) conditions with a reaction time of 1 h, using a cubic anvil-type high-pressure apparatus. The obtained samples were characterized by time-of-flight neutron diffraction experiments using the high-resolution diffractometer Wish at ISIS, UK [34]. Rietveld refinements of the neutron data were carried out using the JANA 2006 software package [35] and crystallographic representation by using VESTA software [36]. DC magnetization and specific heat for the samples were measured using a commercial superconducting quantum interference device magnetometer and Physical Property Measurement System (PPMS) from Quantum Design, using a relaxation technique, respectively. For the dielectric and pyroelectric current measurements, the sample was transformed into a thin disklike pellet coated with high-quality PELCO silver paste at the bottom and top sides to form a parallel plate capacitor. The dimensions of the pellets were $t = 0.294$ mm and $A = 9$ mm^2 for LuFeWO_6 and $t = 0.282$ mm, and $A = 8$ mm^2 for LuCrWO_6. The dielectric constant as a function of temperature was measured at various frequencies and magnetic fields using an LCR meter (Agilent E4980A) integrated with PPMS. Conventional pyroelectric measurements obtained the pyroelectric current and field-induced electric

polarization. The pyroelectric current was measured using an electrometer (Keithley 6517A).

III. COMPUTATIONAL DETAILS

We have performed DFT calculations employing the frozen core projector augmented plane wave [37,38] encoded in VASP [39] and the PBE potential [40] for the exchange-correlation functional. All our calculations used the plane-wave cutoff energy of 450 eV, a set of $(6 \times 6 \times 4)$ k points, and the threshold of 10^{-6} eV for self-consistent-field energy convergence. The electron correlation associated with the $3d$ states of M (= Fe and Cr) was considered by DFT+U calculations with an effective on-site repulsion $U_{\text{eff}} = U - J = 3$ eV [41].

IV. RESULTS

A. Crystal structure

Room temperature x-ray diffraction profiles, collected with a PANalytical Empyrean alpha-1 diffractometer using monochromatized Cu $K\alpha 1$ radiation ($\lambda = 1.5406$ Å), are displayed in Figs. S1 and S2 in the Supplemental Material [42]. Our Le-Bail fitting analysis of these data suggested an orthorhombic cell consistent with the $Pna2_1$ cell of $\text{Lu}M\text{WO}_6$ (M = Fe and Cr). To get the exact positional parameters for the oxygen atoms, as it was difficult to obtain from the laboratory x-ray diffraction data, we carried out neutron diffraction experiments using the high-resolution Wish diffractometer [26].

Figure 1 displays the Rietveld refined neutron diffraction data of $\text{Lu}M\text{WO}_6$ (M = Fe and Cr) recorded at 100 K, confirming that the crystal structure is consistent with the polar orthorhombic $Pna2_1$ symmetry. In addition to the main phase, a trace amount of an unknown impurity phase was detected. The coordination environments around the Fe^{3+}, Cr^{3+}, and W^{6+} ions are presented in Fig. 2, and the positional and thermal parameters obtained from Rietveld refinement of neutron data are respectively given in Tables S1 and S2 in the Supplemental Material [42]. As shown in Fig. 2, the crystal structure consists of dimers of edge-sharing $M\text{O}_6$ (M = Fe or Cr) and WO_6 octahedra. These dimers are connected through corner sharing to form a three-dimensional framework with the Lu^{3+} cations located in the voids between the $M\text{O}_6$ and WO_6 octahedra.

B. Magnetic properties

The thermal evolution of magnetic susceptibility $\chi(T)$ measured using the probe field of 0.1 T and the heat capacity with a magnetic field of 0 T are shown in Figs. 3(a) and 3(b), for LuFeWO_6 and LuCrWO_6, respectively. The magnetic susceptibility data suggest an AFM ordering of the Fe^{3+} spins at 11.8 K and that of the Cr^{3+} spins ~ 19.2 K. The sharp λ-type anomalies in the heat capacity $C_p(T)$ data, shown in the right axis of Figs. 3(a) and 3(b), confirm their long-range magnetic ordering.

The inverse magnetic susceptibility $1/\chi$ vs T data for both compounds are plotted in Fig. S3 in the Supplemental Material [42] and are fitted with the Curie-Weiss law in the paramagnetic regime, as shown by the red solid line. The
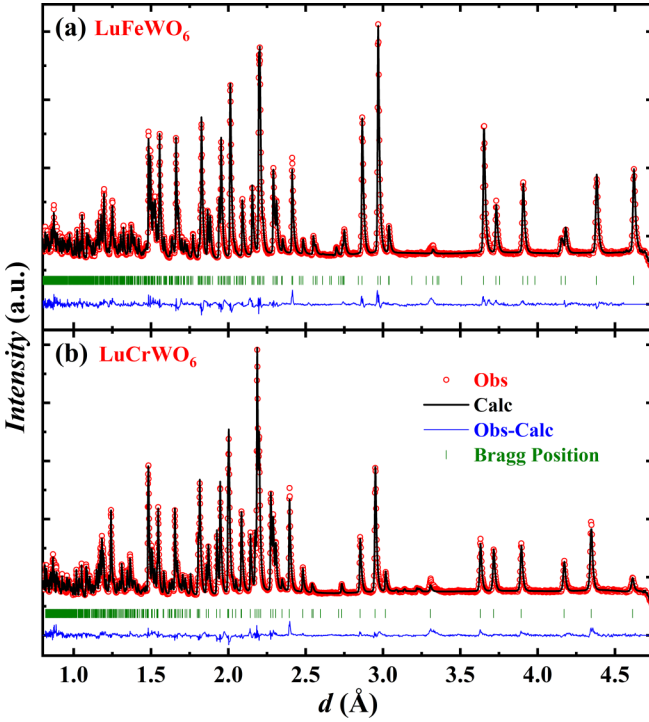
FIG. 1. Rietveld plot of the time-of-flight neutron diffraction pattern of (a) LuFeWO$_6$ and (b) LuCrWO$_6$ recorded at 100 K from the high-resolution Wish bank with an average $2\theta = 152.83°$. The red points indicate the experimental data, whereas the black and blue lines represent the calculated and difference curves. The olive vertical bars indicate the Bragg reflections position of the main phase.

obtained effective paramagnetic moments (μ_{eff}) from the fit are 6.22 and 4.03 μ_B for LuFeWO$_6$ and LuCrWO$_6$, respectively. These are slightly higher than the theoretical values of the Fe^{3+} (5.92μ_B) and Cr^{3+} (3.87 μ_B) ions. In general, the larger-than-expected values could be due to the presence of an unknown impurity or an orbital contribution, but in the present case, the orbital moment contribution would be negligible for the $(t_{2g}\uparrow)^3(e_g\uparrow)^2$ configuration of a high-spin Fe^{3+} ion and the $(t_{2g}\uparrow)^3$ configuration of a high-spin Cr^{3+} ion. The magnetic susceptibility of LuFeWO$_6$ in the paramagnetic region, when fitted by the Curie-Weiss law, leads to the Curie-Weiss temperature (θ_{CW}) of -98.3 K. Thus, the frustration index $f = \theta_{CW}/T_N = 8.33$, indicating a higher degree of spin frustration in LuFeWO$_6$ [43] than LuCrWO$_6$ for which θ_{CW} is found to be -39.26 K, and its frustration index is $f \approx 2.04$. Isothermal $M(H)$ loops measured for LuFeWO$_6$ and LuCrWO$_6$ at various temperatures are shown in Figs. 3(c) and 3(d), consistent with the AFM ordering below T_N and a paramagnetic behavior above T_N. However, the $M(H)$ loops measured below T_N for both compounds exhibit a slight nonlinear behavior with a change in the slope ($\sim$5 T at 2 K). The latter moves to a higher field with increasing temperature [see the dM/dH curves in the inset of Figs. 3(c) and 3(d)]. This behavior indicates the presence of some degree of spin reorientation under the magnetic field below T_N.

For further analysis, the magnetic contribution $C_{mag}(T)$ to the heat capacity of LuFeWO$_6$ and LuCrWO$_6$ is estimated by calculating the phonon contribution [$C_{ph}(T)$] by fitting the

total heat capacity in the temperature range of 40–100 K using the combined Debye-Einstein model, as given by

$$C_{ph}(T) = \frac{9aR}{x_D^3}\int_0^{x_D}\frac{x^4\,e^x}{(e^x-1)^2}dx + R\sum_{i=1}^{24}b_n\frac{x_{E,i}^2\,e^{x_{E,\,i}}}{[e^{x_{E,\,i}}-1]^2},$$

(1)

where R is the universal gas constant, $x_{D,\,E} = \frac{\theta_{D,\,E}}{T}$; θ_D and θ_E are the Debye and Einstein temperatures, respectively. In the Debye-Einstein model, the total number of modes of vibration (acoustic plus optical) is equal to the total number of atoms in the primitive unit cell. In this model, we have considered the ratio of the relative weights of acoustic modes and the sum of the different optical modes to be 1:($n-1$). For both the compounds, therefore, the phonon spectrum consists of a total of 27 vibrational modes, and the data can be fitted well with one Debye term (three acoustic modes) and four Einstein terms (24 optical modes). Several optical modes were grouped using the same Einstein temperature to reduce the number of free parameters and consider the experimental error, and the best fit was obtained for the 3-3-7-11 grouping scheme. The obtained values of θ_D, θ_{E1}, θ_{E2}, θ_{E3}, and θ_{E4} are 192(1), 96(2), 193(3), 571(6), and 380(2) K for LuFeWO$_6$ and 247(1), 120(1), 281(2), 851(9), and 474(2) K for LuCrWO$_6$, respectively. The obtained lattice contribution is extrapolated to 2 K, as shown by the solid red line in Figs. 4(a) and 4(c). The magnetic contribution to the heat capacity $C_{mag}(T)$ therefore can be obtained by subtracting the lattice contribution $C_{ph}(T)$ from total heat capacity, as shown in the insets of Figs. 4(a) and 4(c), for LuFeWO$_6$ and LuCrWO$_6$, respectively.

The magnetic entropy associated with the magnetic transitions for both compounds, calculated by using the equation:

$$\Delta S_{mag}(T) = \int_0^T\frac{C_{mag}(T')}{T'}\,dT',$$

(2)

are shown in Figs. 4(b) and 4(d). The expected value of change in entropy due to magnetic ordering of Fe^{3+} ($S=\frac{5}{2}$) spins is $\Delta S_{mag} = R\ln(2S+1) = 14.90$ J/(mol K) at high temperatures. For LuFeWO$_6$, the observed value $\Delta S_{mag} = 6.88$ J/(mol K) at 100 K is almost half the expected change in entropy. In addition to the fact that this compound shows long-range magnetic ordering, this significant decrease in entropy suggests the presence of magnetic frustration. In contrast, the magnetic entropy for LuCrWO$_6$ saturates at a value of 10.66 J/(mol K), which is close to the theoretical value for Cr^{3+} ions ($S=\frac{3}{2}$), i.e., 11.53 J/(mol K), as expected for the fully ordered spins with negligible frustration.

C. Spin exchange and spin frustration

To understand the difference in spin frustration in the isostructural compounds, we have carried out the DFT calculations. In LuMWO$_6$ (M = Fe and Cr), the spin exchanges between M^{3+} ions are of the $M-O\ldots$W$^{6+}\ldots$O–M type. As depicted in Fig. 5, we consider six different spin exchange paths J_1–J_6 using the spin Hamiltonian defined as

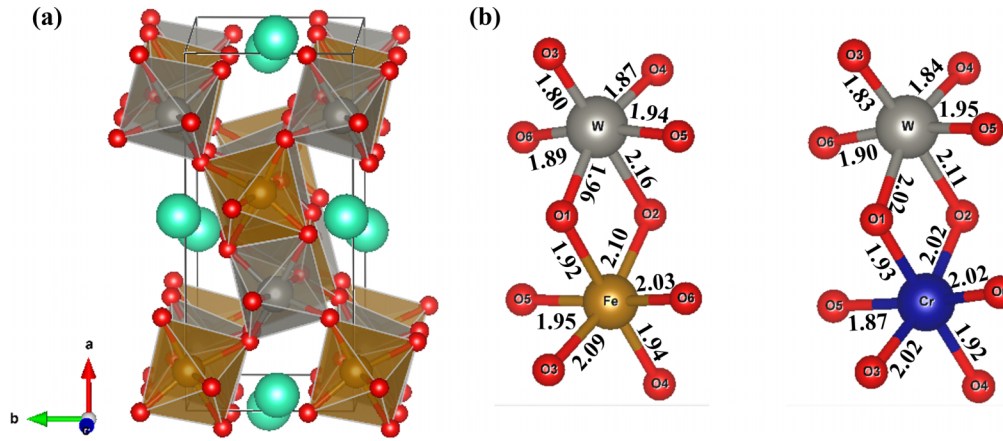$$H_{spin} = \sum_{i>j}J_{ij}\vec{S}_i\cdot\vec{S}_j,$$

(3)

FIG. 2. (a) The ordered aeschynite-type crystal structure of LuMWO$_6$ (M = Fe and Cr) obtained from the refinement of neutron diffraction data. Lutetium (turquoise), transition metal (brown), tungsten (gray), and oxygen (red). (b) Coordination environment of Fe^{3+}/Cr^{3+} and W^{6+} cations by oxygen displaying different Fe/Cr–O and W–O bond lengths in Å.

where $J_{ij} = J_1-J_6$ is the spin exchange constant. To determine the values of J_1-J_6, energy-mapping analysis [44,45] was employed as described in the Supplemental Material [42] based on the seven ordered spin states depicted in Fig. S4 in the Supplemental Material [42]. With the energies of the seven ordered spin states given in terms of the spin exchanges (Table S3 in the Supplemental Material [42]) and the DFT+U calculations (Table S4 in the Supplemental Material [42]), the values of J_1-J_6 obtained from our energy-mapping analyses are summarized in Table I.

The magnetic structures of LuFeWO$_6$ and LuCrWO$_6$ predicted by the DFT+U calculations are presented in Figs. 6(a) and 6(b), respectively. In discussing the essential features of these magnetic structures, it is convenient to describe them in terms of the rectangular lattices defined by J_5 and J_6, which are parallel to the bc plane. In each J_5-J_6 rectangular lattice, adjacent spins are coupled AFM in LuFeWO$_6$ but ferromagnetically (FM) in LuCrWO$_6$. In LuFeWO$_6$, each J_5-J_6 rectangular lattice is AFM because both J_5 and J_6 are substantially AFM. In LuCrWO$_6$, however, each J_5-J_6 rectangular
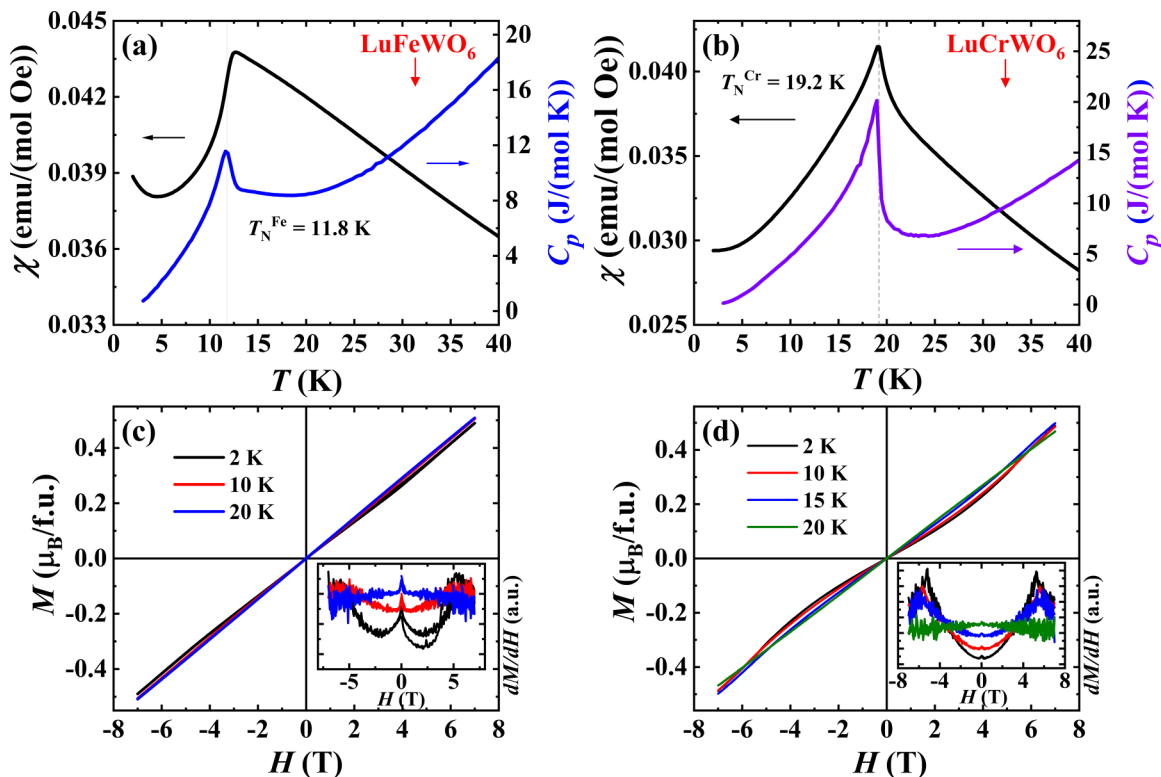

FIG. 3. (a) and (b) Left axis: Temperature dependence of DC magnetic susceptibility measured under a magnetic field of 0.1 T in the field-cooled (FC) condition. Right axis: Temperature dependence of heat capacity measured under zero magnetic field. (c) and (d) Isothermal magnetization curves at different temperatures (insets show dM/dH vs H) for LuFeWO$_6$ and LuCrWO$_6$, respectively.
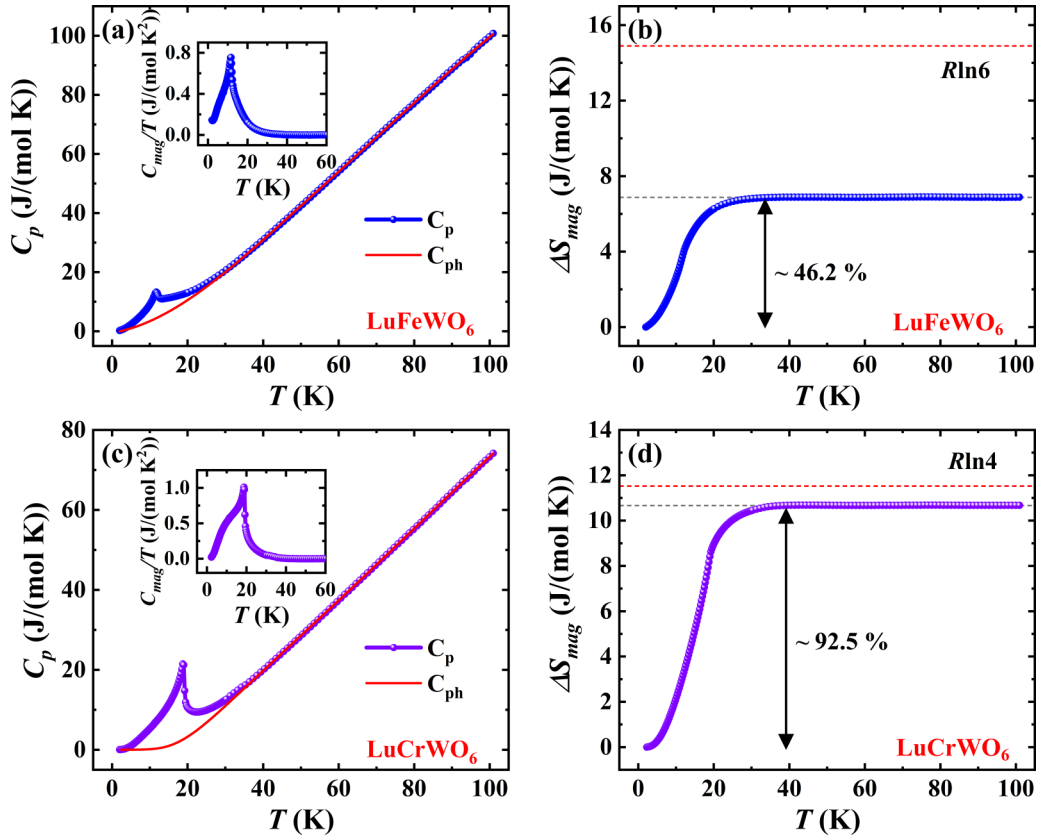
FIG. 4. (a) and (c) Temperature-dependent heat capacity measured in zero magnetic fields. The solid red line is the phonon contribution obtained using the combined Debye-Einstein model [insets show the magnetic contribution to the heat capacity (C_{mag}/T)]. (b) and (d) Magnetic entropy calculated from C_{mag}. The dashed red line represents the total spin entropy for $LuFeWO_6$ and $LuCrWO_6$, respectively.

lattice is FM for the following reasons: First, J_5 is FM, and J_6 is weakly AFM, so the two stronger AFM J_2 paths in each (J_6, J_2, J_2) triangle force the spins of each J_6 path to have FM coupling. In $LuFeWO_6$, adjacent J_5–J_6 rectangular lattices are spin frustrated through the (J_5, J_4, J_3) and (J_5, J_2, J_2) spin exchange triangles, i.e., $(J_5, J_4, J_3)=(2.66, 4.82, 1.55)$ and $(J_5, J_2, J_2)=(2.66, 6.15, 6.15)$. In $LuCrWO_6$, $(J_5, J_4, J_3)=(-2.74, 0.27, -1.20)$ and $(J_5, J_2, J_2)=(-2.74, 3.08, 3.08)$. Thus, the (J_5, J_2, J_2) triangle is not spin frustrated, but the (J_5, J_4, J_3)

triangle is weakly spin frustrated because J_4 is weakly AFM. Consequently, the extent of spin frustration between adjacent J_5–J_6 rectangular lattices is weak in $LuCrWO_6$.

D. Electrical properties

To explore the possibility of the presence of magnetoelectric coupling, we performed dielectric and pyroelectric current measurements on both compounds. The dielectric
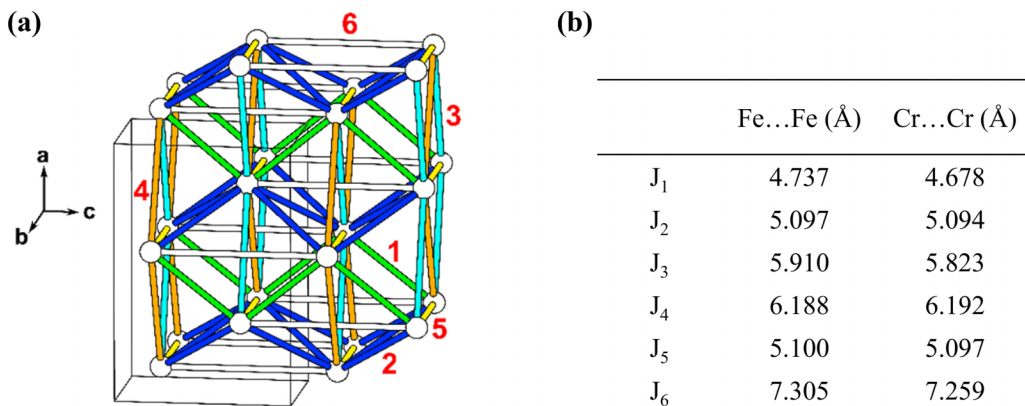
FIG. 5. (a) Arrangement of the spin exchange paths J_1–J_6 in $LuMWO_6$ (M = Fe and Cr), where the numbers 1–6 refer to the spin exchange paths J_1–J_6, respectively. Different spin exchange paths are represented by cylinders of different colors. (b) The $M … M$ distances associated with the exchange paths J_1–J_6.

	Fe…Fe (Å)	Cr…Cr (Å)
J_1	4.737	4.678
J_2	5.097	5.094
J_3	5.910	5.823
J_4	6.188	6.192
J_5	5.100	5.097
J_6	7.305	7.259

TABLE I. Spin exchange parameters (in K) of LuMWO$_6$ ($M =$ Fe and Cr) obtained by DFT$+U$ calculations; $U_{\text{eff}} = 3$ eV.

	LuFeWO$_6$	LuCrWO$_6$
J_1	3.34	3.04
J_2	6.15	3.08
J_3	1.55	-1.20
J_4	4.82	0.27
J_5	2.66	-2.74
J_6	3.77	0.76

properties of LuFeWO$_6$ and LuCrWO$_6$ measured with a constant frequency of 50 kHz under various applied magnetic fields are shown in Fig. 7. We observe an apparent dielectric anomaly around the magnetic ordering temperature, indicating the strong coupling between magnetic and dielectric orders, which is also correlated with the dielectric loss of the sample, as shown in the inset of Fig. 7. The observed dielectric anomaly shifts to a lower temperature as the field is increased. The frequency-dependent dielectric properties of LuFeWO$_6$, measured in the 5–300 kHz frequency range (Fig. S5 in the Supplemental Material [42]), further confirm this correlation. The dielectric anomaly around T_N is frequency independent, so these are not associated with any relaxation phenomena and validate the intrinsic behavior. Moreover, the presence of dielectric dispersion under applied magnetic fields below T_N (see Fig. 7) confirms the significant magnetodielectric (MD) effect in both compounds. Further, as shown in Fig. 7, both compounds exhibit different behaviors of the MD effect. In LuFeWO$_6$, the dielectric anomaly shifts slightly to lower temperatures with a magnetic field like the heat capacity anomaly (see Fig. S6 in the Supplemental Material [42]), resulting in the negative MD effect. On the other hand, in LuCrWO$_6$, the dielectric anomaly at T_N is suppressed under magnetic field. Interestingly, there is a new dielectric anomaly at the second transition, which shifts toward lower temperatures with increasing magnetic field. Consequently, we observe a positive MD effect in LuCrWO$_6$. In addition, the low values of the dielectric loss at 50 kHz imply the high-insulating nature of both compounds at low temperatures. Thus, the dielectric

anomalies at the magnetic ordering temperature indicate a possible magnetoelectric coupling in the present polycrystalline samples.

We investigated the magnetoelectric coupling of LuFeWO$_6$ by recording the pyroelectric current under the absence and presence of different magnetic fields, as displayed in Fig. 8(a). In this pyroelectric current measurement, the sample was cooled from 20 to 2 K (note that $T_N \sim 11.8$ K) under a poling electric field of $+8.5$ kV/cm. Then the sample was cooled down to the lowest temperature 2 K with its electrodes shorted for 20 min to remove stray charges. After this, the pyroelectric current was recorded while warming the sample at 3 K/min from 2 to 20 K under magnetic field strength from 0 to 9 T. Clear asymmetric peaks were observed at the dielectric anomaly temperature, corresponding to the depolarization of a dipole. The electric polarization was obtained and shown in Fig. 8(b) from the time integration of pyroelectric current. Since this compound has a polar structure, there can be a nonzero electric polarization in the paramagnetic region, allowing spontaneous polarization in the direction of the c axis (p_z). However, we did not observe switchable polarization in the paramagnetic region, indicating the pyroelectric feature of this compound. Hence, the additional electric polarization observed below T_N is solely caused by the emergence of a new component along the a axis due to the magnetic ordering of Fe^{3+} ions, which will be discussed in the following section. The magnetic field dependence of polarization is shown in Fig. 8(c), where the polarization is suppressed, suggesting the magnetic structure change under the applied field. It can be noted that the polarization is completely suppressed under low magnetic fields in other compounds of the same family with a magnetic rare earth due to the strong influence of $4f-3d$ interaction [17,22,23]. However, the polarization is not entirely suppressed in the compounds containing nonmagnetic rare earth (Lu and Y) even at high magnetic fields of 9 T [17]. Thus, the development of additional electric polarization at T_N shows that its origin is linked to magnetic ordering, i.e., magnetoelectric coupling. The electric polarization can also be switched with a negative electric field, as shown in Fig. 8(b). Since our samples are polycrystalline, a single-crystal study is required to confirm
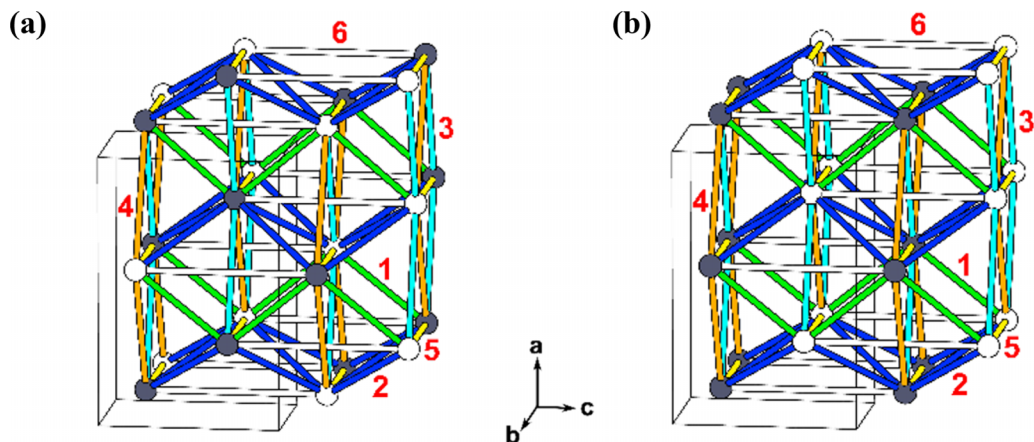

FIG. 6. The lowest-energy spin arrangement predicted by DFT$+U$ calculations for (a) LuFeWO$_6$ and (b) LuCrWO$_6$, where the shaded and unshaded spheres represent the up-spin and down-spin sites, respectively.
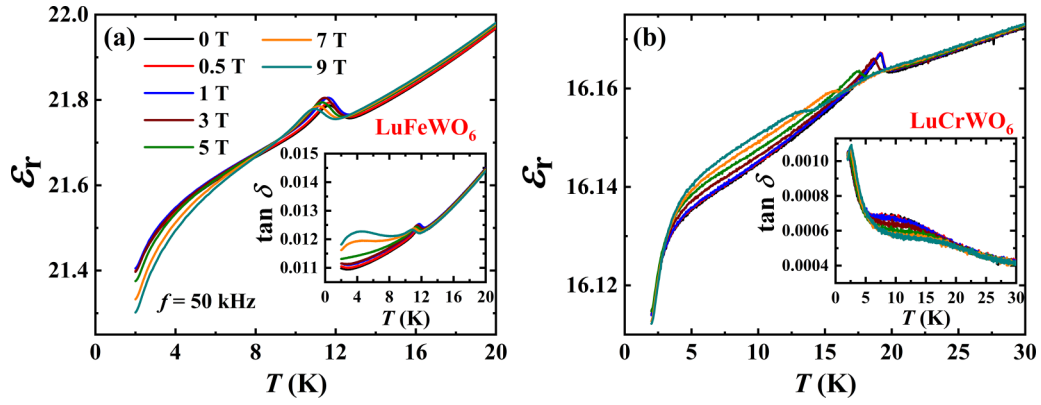
FIG. 7. (a) and (b) Temperature dependence of dielectric constant measured under applying magnetic fields with 50 kHz. The inset shows the corresponding dielectric loss tangent as a function of temperature for $LuFeWO_6$ and $LuCrWO_6$, respectively.

the true nature of the switchability of polarization. Further, the intrinsic nature of magnetoelectric coupling is confirmed by the DC bias current measurements on $LuFeWO_6$ while warming with an electric field of $+8.5$ kV/cm. The results are depicted in Fig. 8(d), where we see a consecutive upward peak due to the polarization of the dipoles followed by a downward peak due to the depolarization at the magnetic ordering temperature.

In contrast to $LuFeWO_6$, the measurements for the presence of magnetoelectric coupling (standard pyroelectric and

DC bias current measurements) in $LuCrWO_6$ did not show an anomaly at T_N, confirming the absence of additional polarization.

E. Magnetic structure of $LuMWO_6$ ($M =$ Fe and Cr)

To unravel the nature of magnetic ordering and understand the magnetoelectric coupling at T_N in $LuMWO_6$ ($M =$ Fe and Cr), we determined the magnetic structures by analyzing the low-temperature neutron diffraction data. $LuFeWO_6$
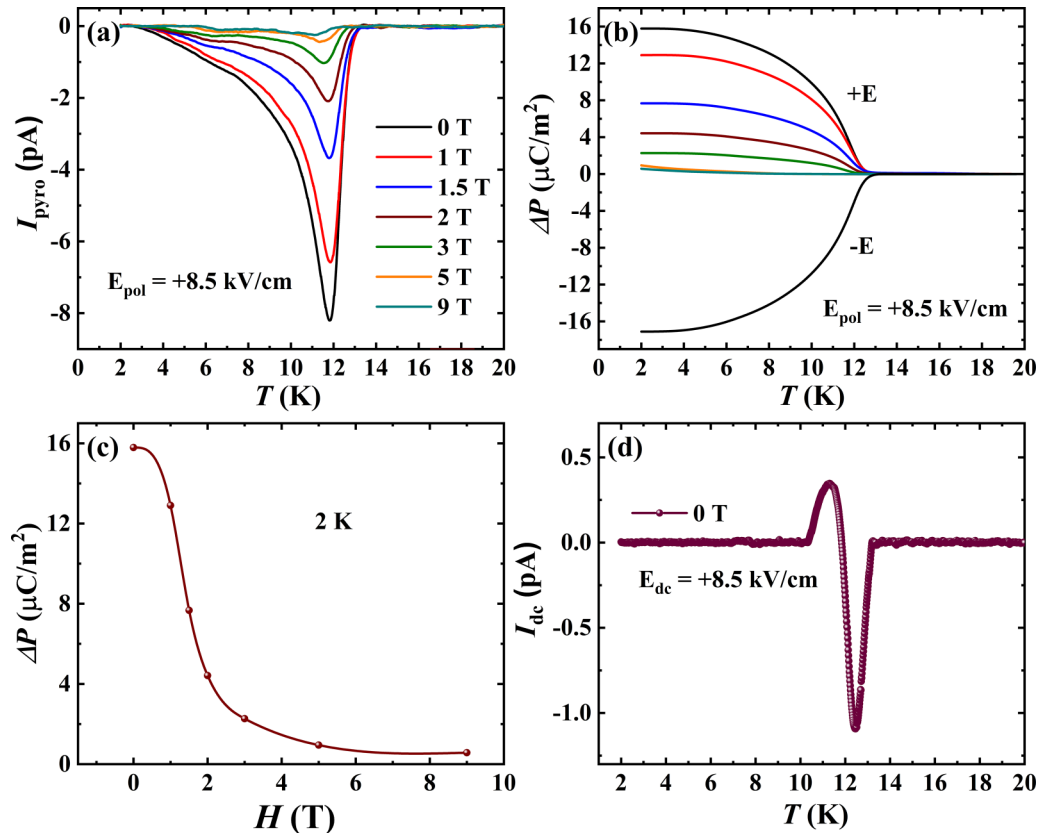

FIG. 8. (a) Temperature dependence of pyroelectric current under $E_{pol} = +8.5$ kV/cm and different magnetic fields. (b) Electric polarization with the temperature at various magnetic fields. (c) The relationship of magnetic field dependence of the electric polarization at 2 K. (d) DC bias at 0 T; for $LuFeWO_6$.
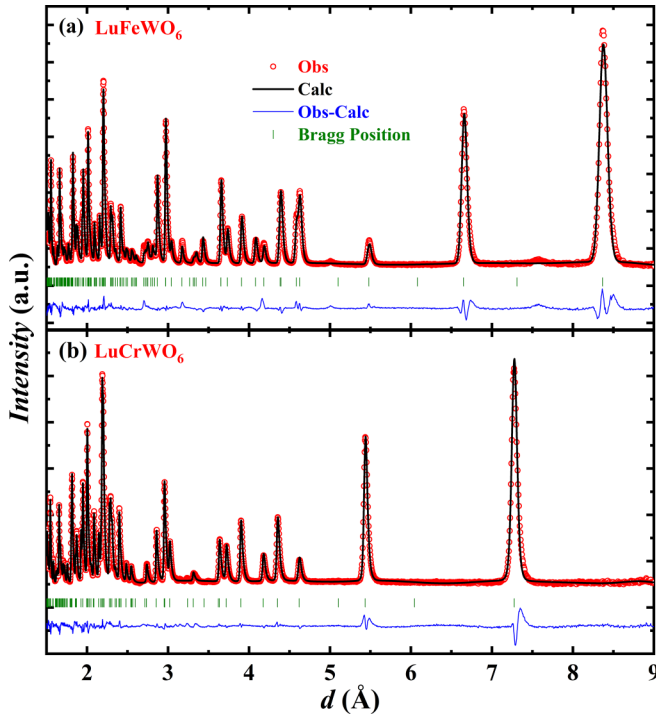
FIG. 9. Rietveld refined neutron diffraction pattern of (a) $LuFeWO_6$ and (b) $LuCrWO_6$ collected at average $2\theta = 58.33°$ at 1.5 K. The red points indicate the experimental data, whereas the black and blue lines represent the calculated and difference curves. The olive vertical bars indicate the Bragg reflection position of the main phase.

magnetic reflections, obtained in the high-resolution diffractometer (Wish), were compatible with the commensurate **k**-vector $(0, \frac{1}{2}, \frac{1}{2})$ reported for $DyFeWO_6$ [17]. To determine the possible magnetic space groups of the ordered phases, using the paramagnetic space group and the **k**-vector, group theoretical calculations were carried out using ISODISTORT [46]. We obtained three isotropy magnetic subgroups, namely, C_ac, P_ac, and P_S1, corresponding to the irreducible representation $mT1$ with different order parameter directions.

The diffraction data collected at 1.5 K (below $T < T_N$) are well modeled with the C_ac magnetic space group, as can be seen from the corresponding Rietveld plot shown in Fig. 9(a). The resulting crystallographic parameters are given in Table II. The refined magnetic structure at 1.5 K, presented in Figs. 10(a) and 10(b), shows that magnetic symmetry splits the paramagnetic Fe crystallographic site into two independent ones, resulting in two magnetic sublattices. In each sublattice, the Fe^{3+} spins are arranged AFM in the bc and ac planes with the two sublattices nearly perpendicular along the a direction; as a result, $LuFeWO_6$ has a strongly noncollinear magnetic structure. This noncollinear structure is likely because the spins of the adjacent $J_5–J_6$ rectangular lattices are strongly spin frustrated, as discussed in the previous section. Further, the point group symmetry associated with the paramagnetic space group $Pna2_1.1'$ is $mm2.1'$, which allows electric polarization along the c direction. As discussed above, the magnetic point group (space group C_ac) obtained from the neutron analysis is $m.1'$. Due to mirror

TABLE II. Crystallographic parameters of $LuFeWO_6$ obtained from Rietveld refinement of neutron diffraction data at 1.5 K. Ordered magnetic moments at selected temperatures are shown at the bottom. All atoms assume full occupancy. Cell dimensions: $a = 14.6102(1)$ Å, $b = 10.1999(1)$ Å, $c = 10.9544(1)$ Å, $\alpha=\beta=\gamma= 90°$, $V = 1632.454(57)$ Å^3; goodness of fit = 4.60, reliability factors: R_p (%)= 3.21, R_{wp} (%)= 4.00.

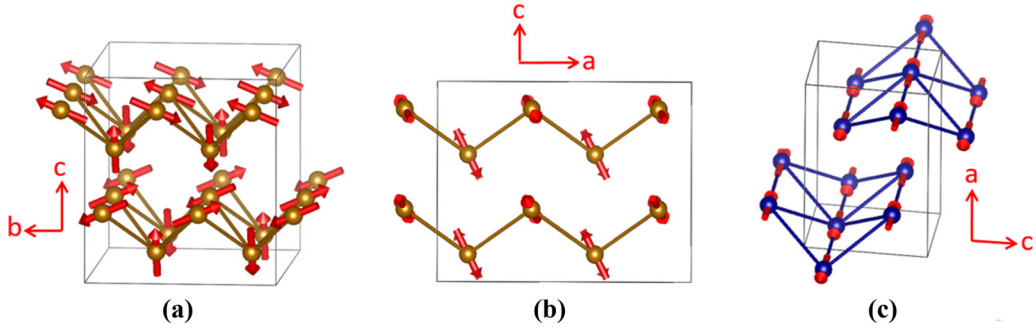| Atom	Wyckoff site	x	y	z	U_{iso} (Å^2)
Lu1	8a	0.7549(14)	0.3961(8)	0.0435(12)	0.0098(5)
Lu2	8a	0.0049(15)	0.3539(7)	−0.0435(11)	0.0098(5)
Fe1	8a	0.6211(14)	0.1411(4)	0.1373(11)	0.0073(6)
Fe2	8a	0.8711(14)	0.1089(5)	0.8627(11)	0.0073(6)
W1	8a	0.6288(16)	0.4024(10)	0.3525(14)	0.0011(8)
W2	8a	0.8788(15)	0.3476(11)	0.6475(15)	0.0011(8)
O1_1	8a	0.6465(15)	0.2401(11)	−0.0266(14)	0.0106(4)
O1_2	8a	0.8965(14)	0.0099(9)	0.0266(12)	0.0106(4)
O2_1	8a	0.6005(16)	0.0032(10)	0.5247(14)	0.0106(4)
O2_2	8a	0.8505(16)	0.2468(10)	0.4753(13)	0.0106(4)
O3_1	8a	0.6599(15)	0.3207(9)	0.2133(12)	0.0106(4)
O3_2	8a	−0.0901(15)	0.4293(7)	0.7867(12)	0.0106(4)
O4_1	8a	0.5906(14)	0.0645(9)	0.2935(13)	0.0106(4)
O4_2	8a	0.8406(14)	0.1856(10)	0.7065(13)	0.0106(4)
O5_1	8a	0.7532(17)	0.0906(10)	0.1433(13)	0.0106(4)
O5_2	8a	0.0032(15)	0.1594(8)	0.8567(12)	0.0106(4)
O6_1	8a	0.4974(16)	0.2193(7)	0.1167(12)	0.0106(4)
O6_2	8a	0.7474(15)	0.0306(8)	0.8833(13)	0.0106(4)
Ordered magnetic moments					
T (K)			$\mu_{Fe^{3+}}(\mu_B)$		
1.5			3.441(4)		
6			3.288(4)		
10			2.633(5)		

FIG. 10. (a) and (b) The observed magnetic structure of $LuFeWO_6$ in perspective and projection views. (c) The observed magnetic structure of $LuCrWO_6$ in a perspective view. In each diagram, the J_2 exchange paths between adjacent spin sites are added as lines to accentuate the three-dimensional nature of the spin arrangement.

plane symmetry, the electric polarization is confined in the ac plane, like $DyFeWO_6$ [17].

In contrast, the magnetic ground state of the isostructural $LuCrWO_6$ is compatible with the commensurate $\mathbf{k}$-vector (0, 0, 0). We found four possible magnetic models corresponding to four irreducible representations, namely, $m\Gamma_1$: $Pna2_1$, $m\Gamma_2$: $Pn'a'2_1$, $m\Gamma_3$: $Pn'a2'_1$, and $m\Gamma_4$: $Pna'2'_1$. The magnetic space group $Pna2_1$ corresponding to the $m\Gamma_1$ irreducible representation correctly describes the magnetic ground state at 1.5 K. The resulting Rietveld plot is shown in Fig. 9(b), and the obtained crystallographic parameters at 1.5 K are given in Table III. The best fit is achieved when the magnetic moments lie along the b direction since the magnitude of the a and c components were negligible. The removal of the latter components did not degrade the refinement, leading to a collinear magnetic configuration with magnetic moments along the b direction, as presented in Fig. 10(c), like that of $DyCrWO_6$ and $HoCrWO_6$ [28,30]. As shown in Fig. 10(c), the Cr^{3+} spins are arranged FM along the b axis, and the FM layers are stacked AFM along the c axis, leading to an A-type AFM configuration. The collinear AFM arrangement of the spins in $LuCrWO_6$ is understandable because the spin frustration

between the adjacent J_5–J_6 rectangular lattices in $LuCrWO_6$ is small. Further, the magnetic point group symmetry $mm2$ (space group $Pna2_1$) allows electric polarization along the c direction, like in the paramagnetic state. However, we do not observe any change in polarization below T_N, indicating the absence of magnetoelectric coupling.

V. DISCUSSION

The absence of switchable polarization in the paramagnetic state of the isostructural polar magnets investigated in this paper indicate that these compounds are pyroelectric. The observation of additional polarization below T_N depends upon the strength of the magnetoelectric coupling, which in turn depends upon the spin arrangement in the sublattice of the transition metal magnetic ions. As discussed above, the spin lattice of $LuFeWO_6$ is spin frustrated, but that of $LuCrWO_6$ is not. This noticeable difference originates ultimately from the difference in the magnetic orbitals of the Fe^{3+} and Cr^{3+} ions. With $(t_{2g} \uparrow)^3 (e_g \uparrow)^2$ configuration for Fe^{3+} ions in $LuFeWO_6$, all five d states of Fe^{3+} are magnetic orbitals. With $(t_{2g} \uparrow)^3$ configuration for the Cr^{3+} ions in $LuCrWO_6$, only the t_{2g}

TABLE III. Crystallographic parameters of $LuCrWO_6$ obtained from Rietveld refinement of neutron diffraction data at 1.5 K. Ordered magnetic moments at selected temperatures are shown at the bottom. All atoms assume full occupancy. Cell dimensions: $a = 10.8575$ (1) Å, $b = 5.0990(1)$ Å, $c = 7.2623(1)$ Å, $\alpha=\beta=\gamma= 90°$, $V = 402.063(12)$ Å^3; goodness of fit = 4.20, reliability factors: R_p (%)= 3.52, R_{wp} (%)= 3.89.

Atom	Wyckoff site	x	y	z	U_{iso} (Å^2)
Lu	$4a$	−0.0443(1)	0.5468(2)	0.4997(4)	0.0207(4)
Cr	$4a$	0.1343(4)	−0.0436(10)	0.2563(8)	0.0115(14)
W	$4a$	0.3521(3)	0.4404(8)	0.2444(7)	0.0306(13)
O1	$4a$	0.0229(3)	0.2484(7)	0.3044(9)	0.0163(11)
O2	$4a$	0.4764(3)	0.7338(7)	0.2156(9)	0.0217(13)
O3	$4a$	0.2124(4)	0.6105(8)	0.1888(8)	0.0350(14)
O4	$4a$	0.2911(3)	0.1242(7)	0.3232(8)	0.0078(9)
O5	$4a$	0.1170(1)	0.8194(2)	0.4964(11)	0.0138(5)
O6	$4a$	0.35742(12)	0.5669(2)	0.4868(9)	0.0109(5)
Ordered magnetic moments					
T (K)			$\mu_{Cr^{3+}}(\mu_B)$		
1.5			2.507(9)		
6			2.457(9)		
12			2.176(9)		

states of Cr^{3+} are magnetic orbitals. The $3d$ orbitals of M make π-antibonding with the $2p$ orbitals of the surrounding O ligands in the t_{2g} states but σ-antibonding in the e_g states [44,45]. Furthermore, the e_g magnetic orbitals give rise to stronger AFM interactions for the $M-O \ldots W^{6+} \ldots O-M$ spin exchange than do t_{2g} magnetic orbitals [44,45]. In short, $LuFeWO_6$ adopts a noncollinear magnetic structure to reduce spin frustration arising from the e_g magnetic orbitals. In contrast, $LuCrWO_6$ has a collinear spin structure since its e_g orbitals are not magnetic orbitals.

A detailed symmetry analysis of the magnetic transition of $LuMWO_6$ can give extra insight regarding the observation or not of a switchable polarization below T_N. The ordered aeschynite structure can be derived from the simple one ($CaTa_2O_6$, space group $Pnma.1'$) by the action of the one-dimensional irrep Γ_4^-. The ordering of the cations in the $8d$ site of the $Pnma.1'$ structure is the primary order parameter, and it will induce a polar displacive distortion, which transforms as the same Γ_4^- irreps along the c direction. This induced polarization can be switched only if the cation ordering is inverted, which is not physically possible at relatively low temperatures, confirming the pyroelectric character of these compounds in their paramagnetic state. The fact that the cation ordering cannot be changed at a temperature close to T_N for both compounds justifies the assumption of the $Pna2_1.1'$ cation-ordered structure as the parent structure for the symmetry analysis of the magnetic state. The magnetic structure of $LuFeWO_6$ transforms as the mT_1 irreps of the $Pna2_1.1'$ space group with order parameter direction $(\mu, 0)$, which results in the monoclinic $C_a c$ magnetic space group. As highlighted in the previous section, the magnetic transition reduces the point symmetry from $mm2.1'$ to $m.1'$ and, in principle, allows the polarization to move from the parent c-axis direction to the ac plane. This extra component of the polarization transforms as the Γ_4 irreps of the parent group with order parameter δ, and it can be seen as a secondary order parameter induced by the magnetic ordering through the free energy invariant $\delta\mu^2$. This magnetically induced component of the electrical polarization is directed along the a axis of the parent orthorhombic structure, and since it is not linked to the cation ordering, this component can be switched by the application of an external electric field, and this is confirmed by the polarization measurement presented in this paper. From a microscopic point of view, the observed polarization could be due to exchange striction or induced through the spin current or inverse DM interaction mechanism since the strongly noncollinear structure is observed by neutron diffraction. In the Cr compound, the magnetic structure transforms as the

$m\Gamma_1$ irreps with order parameter ζ. In this case, the primary magnetic order parameter does not induce any displacive distortion apart from the total symmetric ones, which transform as the Γ_1 irrep. This has the consequence that, at the magnetic transition, only a change in the amplitude of the polarization can be observed (due to magnetostriction) but no switching of the polarization. However, we do not see a change in polarization at T_N, indicating that the magnetostriction in this compound is very small to induce a change in polarization.

Further, it can be noted that the presence of magnetoelectric coupling in $RFeWO_6$ (R = rare earth) compounds with nonmagnetic rare-earth Y [17] and Lu (this paper) indicates the emergence of additional electric polarization is solely due to the long-range magnetic ordering of Fe^{3+} moments. It implies magnetic rare-earth cations do not play any pivotal role in inducing electric polarization below T_N in $RFeWO_6$ compounds, but R-ion moments affect the magnitude of electric polarization under applied magnetic fields through the $4f-3d$ interaction.

VI. CONCLUSIONS

$LuMWO_6$ (M = Fe and Cr) crystallizes in a polar orthorhombic structure due to the chemical ordering of Fe^{3+} and W^{6+} ions. $LuFeWO_6$ undergoes a noncollinear AFM ordering at $T_N = 11.8$ K, and $LuCrWO_6$ a collinear AFM ordering at $T_N = 19.2$ K. However, the noncollinear AFM ordering induces magnetoelectric coupling in $LuFeWO_6$ through an additional polarization, while the collinear AFM ordering in $LuCrWO_6$ does not. Our calculations show that $LuFeWO_6$ is spin frustrated, but $LuCrWO_6$ is not. Thus, ΔP in $LuFeWO_6$ and its absence in $LuCrWO_6$ suggest that the noncollinear spin structure arising from spin frustration is crucial for the magnetoelectric coupling in $LuFeWO_6$.

[1] D. Khomskii, Classifying multiferroics: Mechanisms and effects, Physics **2**, 20 (2009).

[2] C. N. R. Rao and C. R. Serrao, New routes to multiferroics, J. Mater. Chem. **17**, 4931 (2007).

[3] R. Saha, A. Sundaresan, and C. N. R. Rao, Novel features of multiferroic and magnetoelectric ferrites and chromites exhibiting magnetically driven ferroelectricity, Mater. Horiz. **1**, 20 (2014).

[4] Y. Tokura, S. Seki, and N. Nagaosa, Multiferroics of spin origin, Rep. Prog. Phys. **77**, 76501 (2014).

[5] D. I. Khomskii, Multiferroics: Different ways to combine magnetism and ferroelectricity, J. Magn. Magn. Mater. **306**, 1 (2006).

[6] T. Kimura, T. Goto, H. Shintani, K. Ishizaka, T. Arima, and Y. Tokura, Magnetic control of ferroelectric polarization, Nature (London) **426**, 55 (2003).

[7] S.-W. Cheong and M. Mostovoy, Multiferroics: A magnetic twist for ferroelectricity, Nat. Mater. **6**, 13 (2007).

[8] M.-R. Li, D. Walker, M. Retuerto, T. Sarkar, J. Hadermann, P. W. Stephens, M. Croft, A. Ignatov, C. P. Grams, J. Hemberger *et al.*, Polar and magnetic Mn_2FeMO_6 ($M =$ Nb, Ta) with $LiNbO_3-$type structure: High-pressure synthesis, Angew. Chem., Int. Ed. **52**, 8406 (2013).

[9] M.-R. Li, P. W. Stephens, M. Retuerto, T. Sarkar, C. P. Grams, J. Hemberger, M. C. Croft, D. Walker, and M. Greenblatt, Designing polar and magnetic oxides: Zn_2FeTaO_6—In search of multiferroics, J. Am. Chem Soc. **136**, 8508 (2014).

[10] M.-R. Li, E. E. McCabe, P. W. Stephens, M. Croft, L. Collins, S. V. Kalinin, Z. Deng, M. Retuerto, A. Sen Gupta, H. Padmanabhan *et al.*, Magnetostriction-polarization coupling in multiferroic Mn_2MnWO_6, Nat. Commun. **8**, 2037 (2017).

[11] V. Caignaert, A. Maignan, K. Singh, Ch. Simon, V. Pralong, B. Raveau, J. F. Mitchell, H. Zheng, A. Huq, and L. C. Chapon, Gigantic magnetic-field-induced polarization and magnetoelectric coupling in a ferrimagnetic oxide $CaBaCo_4O_7$, Phys. Rev. B **88**, 174403 (2013).

[12] Y. Wang, G. L. Pascut, B. Gao, T. A. Tyson, K. Haule, V. Kiryukhin, and S.-W. Cheong, Unveiling hidden ferrimagnetism and giant magnetoelectricity in polar magnet $Fe_2Mo_3O_8$, Sci. Rep. **5**, 12268 (2015).

[13] T. Kurumaji, S. Ishiwata, and Y. Tokura, Doping-Tunable Ferrimagnetic Phase with Large Linear Magnetoelectric Effect in a Polar Magnet $Fe_2Mo_3O_8$, Phys. Rev. X **5**, 031034 (2015).

[14] T. Kurumaji, S. Ishiwata, and Y. Tokura, Diagonal magnetoelectric susceptibility and effect of Fe doping in the polar ferrimagnet $Mn_2Mo_3O_8$, Phys. Rev. B **95**, 045142 (2017).

[15] Y. S. Tang, S. M. Wang, L. Lin, C. Li, S. H. Zheng, C. F. Li, J. H. Zhang, Z. B. Yan, X. P. Jiang, and J.-M. Liu, Collinear magnetic structure and multiferroicity in the polar magnet $Co_2Mo_3O_8$, Phys. Rev. B **100**, 134112 (2019).

[16] G.-H. Cai, M. Greenblatt, and M.-R. Li, Polar magnets in double corundum oxides, Chem. Mater. **29**, 5447 (2017).

[17] S. Ghara, E. Suard, F. Fauth, T. T. Tran, P. S. Halasyamani, A. Iyo, J. Rodríguez-Carvajal, and A. Sundaresan, Ordered aeschynite-type polar magnets RFeWO$_6$ (R = Dy, Eu, Tb, and Y): A new family of type-II multiferroics, Phys. Rev. B **95**, 224416 (2017).

[18] C. De and A. Sundaresan, Nonswitchable polarization and magnetoelectric coupling in the high-pressure synthesized doubly ordered perovskites $NaYMnWO_6$ and $NaHoCoW_6$, Phys. Rev. B **97**, 214418 (2018).

[19] R. Shankar P N, S. Mishra, and A. Sundaresan, Polar magnetic oxides from chemical ordering: A new class of multiferroics, APL Mater. **8**, 040906 (2020).

[20] Y. S. Oh, S. Artyukhin, J. J. Yang, V. Zapf, J. W. Kim, D. Vanderbilt, and S.-W. Cheong, Non-hysteretic colossal magnetoelectricity in a collinear antiferromagnet, Nat. Commun. **5**, 3201 (2014).

[21] R. Shankar P N, F. Orlandi, P. Manuel, W. Zhang, P. S. Halasyamani, and A. Sundaresan, A-site and B-site cation ordering induces polar and multiferroic behavior in the perovskite $NaLnNiWO_6$ ($Ln =$ Y, Dy, Ho, and Yb), Chem. Mater. **32**, 5641 (2020).

[22] P. Yanda, S. Mishra, and A. Sundaresan, Magnetic-order-induced ferroelectric polarization in the polar antiferromagnets RFeWO$_6$ ($R =$ Sm, Gd, Er, and Tm), Phys. Rev. Mater. **5**, 074406 (2021).

[23] M. Adnani, M. Gooch, L. Deng, S. Agrestini, J. Herrero-Martin, H.-C. Wu, C.-K. Chang, T. Salavati-fard, N. Poudel, J. L. García-Muñoz *et al.*, Magnetocapacitance effect and magnetoelectric coupling in type-II multiferroic $HoFeWO_6$, Phys. Rev. B **103**, 094110 (2021).

[24] Y. S. Tang, G. Z. Zhou, L. Lin, R. Chen, J. F. Wang, C. L. Lu, L. Huang, J. H. Zhang, Z. B. Yan, X. M. Lu *et al.*, Successive electric polarization transitions induced by high magnetic field in the single-crystal antiferromagnet $Co_2Mo_3O_8$, Phys. Rev. B **105**, 064108 (2022).

[25] H. J. Koo, R. Shankar, F. Orlandi, A. Sundaresan, and M. H. Whangbo, On ferro- and antiferro-spin-density waves describing the incommensurate magnetic structure of $NaYNiWO_6$, Inorg. Chem. **59**, 17856 (2020).

[26] D. P. Panda, P. Yanda, S. S. Behera, and A. Sundaresan, Magnetic, magnetodielectric, and magnetocaloric properties of new polar oxides RCrWO$_6$ ($R =$ Sm, Eu, Gd, and Tb), Solid State Commun. **353**, 114843 (2022).

[27] P. Yanda and A. Sundaresan, Magnetism, magnetocaloric and magnetodielectric properties of $DyVWO_6$: A new aeschynite-type polar antiferromagnet, Mater. Res. Express **6**, 124007 (2020).

[28] C. Dhital, D. Pham, T. Lawal, C. Bucholz, A. Poyraz, Q. Zhang, R. Nepal, R. Jin, and R. Rai, Crystal and magnetic structure of polar oxide $HoCrWO_6$, J. Magn. Magn. Mater. **514**, 167219 (2020).

[29] S. W. Kim, X. Tan, C. E. Frank, Z. Deng, H. Wang, L. Collins, S. H. Lapidus, C. Jin, V. Gopalan, S. V. Kalinin *et al.*, High-pressure, high-temperature synthesis and characterization of polar and magnetic $LuCrWO_6$, Inorg. Chem. **59**, 3579 (2020).

[30] S. Ghara, F. Fauth, E. Suard, J. Rodriquez-Carvajal, and A. Sundaresan, Synthesis, structure, and physical properties of the polar magnet $DyCrWO_6$, Inorg. Chem. **57**, 12827 (2018).

[31] S. W. Kim, T. J. Emge, Z. Deng, R. Uppuluri, L. Collins, S. H. Lapidus, C. U. Segre, M. Croft, C. Jin, V. Gopalan *et al.*, $YCrWO_6$: Polar and magnetic oxide with $CaTa_2O_6$-related structure, Chem. Mater. **30**, 1045 (2018).

[32] R. Salmon, H. Baudry, J. Grannec, and G. L. Flem, Sur de nouvelles séries de composés du tungstène +IV de type aeschynite, Rev. Chim. Miner. **11**, 71 (1974).

[33] L. Jahnberg, Crystal structure of orthorhombic $CaTa_2O_6$, Acta Chem. Scand. **71**, 2548 (1963).

[34] L. C. Chapon, P. Manuel, P. G. Radaelli, C. Benson, L. Perrott, S. Ansell, N. J. Rhodes, D. Raspino, D. Duxbury, E. Spill *et al.*, Wish: The new powder and single crystal magnetic diffractometer on the second target station, Neutron News **22**, 22 (2011).

[35] V. Petříček, M. Dušek, and L. Palatinus, Crystallographic computing system JANA2006: General features, Z. Kristallogr. Cryst. Mater. **229**, 345 (2014).

[36] K. Momma and F. Izumi, VESTA: A three-dimensional visualization system for electronic and structural analysis, J. Appl. Crystallogr. **41**, 653 (2008).

[37] P. E. Blöchl, Projector augmented-wave method, Phys. Rev. B **50**, 17953 (1994).

[38] G. Kresse and D. Joubert, From ultrasoft pseudopotentials to the projector augmented-wave method, Phys. Rev. B **59**, 1758 (1999).

[39] G. Kresse and J. Furthmüller, Efficient iterative schemes for *ab initio* total-energy calculations using a plane-wave basis set, Phys. Rev. B **54**, 11169 (1996).

[40] J. P. Perdew, K. Burke, and M. Ernzerhof, Generalized Gradient Approximation Made Simple, Phys. Rev. Lett. **77**, 3865 (1996).

[41] S. Dudarev and G. Botton, Electron-energy-loss spectra and the structural stability of nickel oxide: An LSDA+U study, Phys. Rev. B **57**, 1505 (1998).

[42] See Supplemental Material at http://link.aps.org/supplemental/10.1103/PhysRevB.108.014435 for x-ray diffraction analysis, inverse susceptibility, energy mapping analysis, and dielectric measurements.

[43] J. E. Greedan, Geometrically frustrated magnetic materials, J. Mater. Chem. **11**, 37 (2001).

[44] H. Xiang, C. Lee, H. J. Koo, X. Gong, and M. H. Whangbo, Magnetic properties and energy-mapping analysis, Dalton Trans. **42**, 823 (2013).

[45] M.-H. Whangbo and H. Xiang, Magnetic properties from the perspectives of electronic Hamiltonian: Spin exchange parameters, spin orientation, and spin-half misconception, in *Handbook of Solid State Chemistry*, edited by R. Dronskowski, S. Kikkawa, and A. Stein (Wiley-VCH Verlag GmbH & Co. KGaA, Weinheim, 2017), pp. 285–343.

[46] B. J. Campbell, H. T. Stokes, D. E. Tanner, and D. M. Hatch, ISODISPLACE: A web-based tool for exploring structural distortions, J. Appl. Crystallogr. **39**, 607 (2006).